Journal of Non-Newtonian Fluid Mechanics, 32 (1989) 253–268
Elsevier Science Publishers B.V., Amsterdam – Printed in The Netherlands

CO-CURRENT AXISYMMETRIC FLOW IN COMPLEX GEOMETRIES: NUMERICAL SIMULATION

S. MUSARRA and R. KEUNINGS *

Center for Advanced Materials, Lawrence Berkeley Laboratory, and Department of Chemical Engineering, University of California, Berkeley CA 94720 (U.S.A.)

(Received December 7, 1988; in revised form January 17, 1989)

Summary

We describe a finite element algorithm for computing steady-state stratified flows of two immiscible viscoelastic fluids in complex geometries. The method is applied to the analysis of co-current axisymmetric flow of both Newtonian and Oldroyd-B fluids through an abrupt expansion or contraction. Good agreement is found between the numerical predictions and experimental data reported by Van de Griend and Denn in the companion paper preceding this one. Predictions at high elasticity levels beyond the range of the experimental data reveal important kinematical differences relative to the Newtonian case.

1. Introduction

The numerical analysis of co-current flow of immiscible viscous liquids in complex geometries is of great practical significance as it relates to polymer processing operations such as co-extrusion and co-injection molding. Finite element techniques for computing the flow of a single Newtonian fluid have been adapted recently to the case of multi-Newtonian fluid systems by Mitsoulis [1], Mavridis et al. [2], Binding et al. [3], and Dheur and Crochet [4]. The major difficulty in the Newtonian case lies in the determination of the interface separating adjacent fluid layers. Interface locations are un-

* Permanent address: Unité de Mécanique Appliquée, Université Catholique de Louvain, Place du Levant 2, 1348 Louvain-la-Neuve, Belgium.

0377-0257/89/$03.50

known *a priori*, which renders the mathematical problem non-linear even for Stokesian flow. The numerical approaches adopted in the literature draw heavily on well known algorithms proposed by Nickell et al. [5] and Kistler and Scriven [6] for extrusion flow simulations.

The present paper is devoted to the numerical simulation of steady-state co-flow of two immiscible viscoelastic fluids in complex geometries. Single-viscoelastic fluid flow computation has been the subject of much research work over the last ten years (see the reviews by Keunings [7] and Crochet [8]). Evident progress has been achieved recently in that a number of viscoelastic simulations are now possible at elasticity levels relevant to polymer processing operations. Difficult challenges remain, however, notably in the numerical treatment of stress singularities and of the mathematical change of type of the governing equations, as well as in the selection of appropriate constitutive models and boundary conditions.

We describe here a finite element technique for computing the flow of two immiscible Oldroyd-B fluids. The method is an extension of a mixed Galerkin finite element technique designed for single fluid calculations (see e.g. Crochet and Keunings [9]). Appropriate finite elements are developed for handling the dynamic conditions at the interface, and both Picard [5] and Newton–Raphson [6] iterative schemes are considered for solving the set of discretized equations. We apply the numerical scheme to the prediction of co-current axisymmetric flow of both Newtonian and viscoelastic liquids through a sudden expansion or contraction. The results are compared to experimental observations reported by Van de Griend and Denn [10] in a companion paper. Predictions at high elasticity levels reveal important kinematical differences relative to the Newtonian case. Similar predictions have been reported recently by Dheur and Crochet [11] using a different numerical approach.

2. Governing equations

We consider steady-state co-flows of two immiscible Newtonian or viscoelastic fluids. In order to identify each fluid phase, we use the superscript α taking the values 1 and 2. Let Ω^α be the flow domain occupied by fluid α; the interface between the two fluids is denoted by Γ (Fig. 1). The momentum and continuity equations for an incompressible fluid hold on Ω^α, i.e.

$$\rho \frac{D\boldsymbol{v}^\alpha}{Dt} = \nabla \cdot \boldsymbol{\sigma}^\alpha + \rho^\alpha \boldsymbol{g}, \qquad \boldsymbol{x} \in \Omega^\alpha, \tag{1}$$

$$\nabla \cdot \boldsymbol{v}^\alpha = 0, \qquad \boldsymbol{x} \in \Omega^\alpha. \tag{2}$$

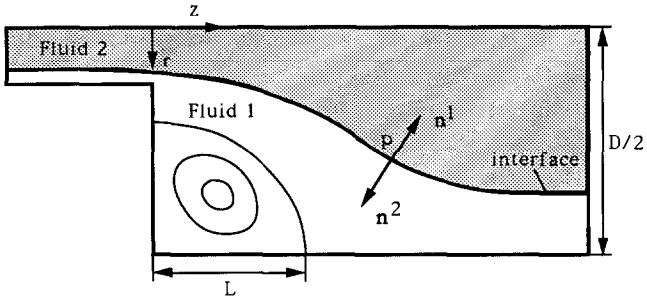

Fig. 1. Schematic of co-flow through an abrupt expansion or contraction.

Here, $\boldsymbol{v}^\alpha$ is the velocity vector, $\boldsymbol{\sigma}^\alpha$ is the Cauchy stress tensor and ρ^α is the density for fluid α; the operator $\mathrm{D}/\mathrm{D}t$ is the material time derivative $\boldsymbol{v}^\alpha \cdot \nabla$. The experimental fluids used by Van de Griend and Denn [10] were modeled either as Newtonian or Oldroyd-B liquids. In the Newtonian case, we have

$$\boldsymbol{\sigma}^\alpha = -p^\alpha \boldsymbol{I} + 2\eta^\alpha \boldsymbol{D}^\alpha, \tag{3}$$

where p^α is the pressure, η^α is the constant shear viscosity, $\boldsymbol{I}$ is the unit tensor and $\boldsymbol{D}^\alpha$ is the rate of strain tensor $\frac{1}{2}(\nabla \boldsymbol{v}^\alpha + \nabla \boldsymbol{v}^{\alpha\mathrm{T}})$. The constitutive equations for an Oldroyd-B fluid are given by

$$\boldsymbol{\sigma}^\alpha = -p^\alpha \boldsymbol{I} + \boldsymbol{\tau}^\alpha, \tag{4}$$

$$\boldsymbol{\tau}^\alpha + \lambda_\mathrm{p}^\alpha \frac{\delta \boldsymbol{\tau}^\alpha}{\delta t} = 2\eta^\alpha \left[\boldsymbol{D}^\alpha + \lambda_\mathrm{r}^\alpha \frac{\delta \boldsymbol{D}^\alpha}{\delta t} \right], \tag{5}$$

where $\lambda_\mathrm{p}^\alpha$ is the polymer relaxation time, $\lambda_\mathrm{r}^\alpha$ is the retardation time and the operator $\delta/\delta t$ is the upper-convected time derivative, i.e.

$$\frac{\delta \boldsymbol{\tau}^\alpha}{\delta t} = \frac{\mathrm{D}\boldsymbol{\tau}^\alpha}{\mathrm{D}t} - \nabla \boldsymbol{v}^{\alpha T} \cdot \boldsymbol{\tau}^\alpha - \boldsymbol{\tau}^\alpha \cdot \nabla \boldsymbol{v}^\alpha. \tag{6}$$

For numerical purposes, it is useful to rewrite the Oldroyd-B model (5) in the equivalent form [9]:

$$\boldsymbol{\tau}^\alpha = \boldsymbol{\tau}_1^\alpha + \boldsymbol{\tau}_2^\alpha, \tag{7}$$

$$\boldsymbol{\tau}_1^\alpha + \lambda_\mathrm{p}^\alpha \frac{\delta \boldsymbol{\tau}_1^\alpha}{\delta t} = 2\eta_\mathrm{p}^\alpha \boldsymbol{D}^\alpha, \tag{8}$$

$$\boldsymbol{\tau}_2^\alpha = 2\eta_\mathrm{s}^\alpha \boldsymbol{D}^\alpha, \tag{9}$$

where

$$\eta^\alpha = \eta_\mathrm{p}^\alpha + \eta_\mathrm{s}^\alpha, \qquad \lambda_\mathrm{r}^\alpha = \lambda_\mathrm{p}^\alpha \eta_\mathrm{s}^\alpha / \eta^\alpha. \tag{10}$$

The partial stresses τ_1^α and τ_2^α are usually referred to as the polymer and solvent components of the extra-stress, respectively.

We complete the mathematical formulation of co-flows with interface conditions. Let $\partial\Omega^\alpha$ denote the boundary of flow domain Ω^α, oriented counterclockwise. At a point P of the interface Γ, we define the outward unit normal and the unit tangent to $\partial\Omega^\alpha$ as $\boldsymbol{n}^\alpha$ and $\boldsymbol{s}^\alpha$, respectively (Fig. 1). In steady-state problems, there is no fluid flow across the interface. This leads to the kinematic condition

$$\boldsymbol{v}^\alpha \cdot \boldsymbol{n}^\alpha = 0, \qquad \boldsymbol{x} \in \Gamma. \tag{11}$$

Assuming there is no relative slip between the two fluids at the interface, we also have

$$\boldsymbol{v}^1 = \boldsymbol{v}^2, \qquad \boldsymbol{x} \in \Gamma. \tag{12}$$

The contact force per unit area acting on fluid α at point P is given by

$$\boldsymbol{t}^\alpha = \boldsymbol{\sigma}^\alpha \cdot \boldsymbol{n}^\alpha. \tag{13}$$

Equilibrium of the interface in the absence of surface tension effects requires that

$$\boldsymbol{t}^1 = -\boldsymbol{t}^2, \qquad \boldsymbol{x} \in \Gamma. \tag{14}$$

It should be pointed out that condition (14) does not necessarily imply continuity of the extra-stress components and pressure across the interface. This important feature of co-flows is taken into account in the numerical scheme.

3. Numerical method

The numerical technique is based on a mixed Galerkin finite element discretization of the flow domain, interface and field variables. The entire flow domain $\Omega = \Omega^1 \cup \Omega^2$ is covered by a mesh of finite elements such that the initially guessed interface coincides with element sides. The unknown field variables τ_1^α, $\boldsymbol{v}^\alpha$ and p^α are discretized by means of nodal values and finite element shape functions, i.e.

$$\boldsymbol{v}^\alpha = \sum_i \boldsymbol{v}_i^\alpha \phi_i(\boldsymbol{x}), \quad \tau_1^\alpha = \sum_j \tau_{1_j}^\alpha \Psi_j(\boldsymbol{x}), \quad p^\alpha = \sum_k p_k^\alpha \pi_k(\boldsymbol{x}), \qquad \boldsymbol{x} \in \Omega^\alpha. \tag{15}$$

We substitute the approximations (15) into the governing equations (1), (2) and (8), and apply Galerkin's principle in order to obtain algebraic equa-

tions for the nodal values. This standard procedure yields [7]

$$\sum_{\alpha} \int_{\Omega^\alpha} \left[\left(\rho^\alpha \frac{\mathrm{D}\boldsymbol{v}^\alpha}{\mathrm{D}t} - \rho^\alpha \boldsymbol{g} \right) \phi_i + \nabla \phi_i^{\mathrm{T}} \cdot \left(-p^\alpha \boldsymbol{I} + 2\eta_{\mathrm{s}}^\alpha \boldsymbol{D}^\alpha + \boldsymbol{\tau}_1^\alpha \right) \right] \mathrm{d}\Omega^\alpha$$

$$= \int_{\partial\Omega} \phi_i \boldsymbol{\sigma}^\alpha \cdot \boldsymbol{n}^\alpha \, \mathrm{d}\, \partial\Omega, \tag{16}$$

$$\sum_{\alpha} \int_{\Omega^\alpha} \Psi_j \left[\boldsymbol{\tau}_1^\alpha + \lambda_{\mathrm{p}}^\alpha \frac{\delta \boldsymbol{\tau}_1^\alpha}{\delta t} - 2\eta_{\mathrm{p}}^\alpha \boldsymbol{D}^\alpha \right] \mathrm{d}\Omega^\alpha = \boldsymbol{0}, \tag{17}$$

$$\sum_{\alpha} \int_{\Omega^\alpha} \pi_k [\nabla \cdot \boldsymbol{v}^\alpha] \, \mathrm{d}\Omega^\alpha = 0, \tag{18}$$

where $\boldsymbol{n}$ is the outward unit normal to the boundary $\partial\Omega$.
If fluid α is Newtonian, we set $\eta_{\mathrm{s}}^\alpha = \eta^\alpha$ and $\lambda_{\mathrm{p}}^\alpha = \eta_{\mathrm{p}}^\alpha = 0$ in (16) and (17); this defines the classical velocity–pressure formulation of Newtonian flow. Alternatively, we can set $\lambda_{\mathrm{p}}^\alpha = 0$ and $\eta_{\mathrm{p}}^\alpha \neq 0$, which defines a mixed method [7]. Both formulations have been used in the present work with virtually identical results. We use isoparametric nine-node quadrilateral and six-node triangular elements to discretize the flow domain Ω. The interface Γ is thus discretized by means of one-dimensional quadratic elements. We select second-order polynomials of class C^0 for the velocity and extra-stress shape functions. The continuity condition (12) is thus automatically satisfied. Since the extra-stress $\boldsymbol{\tau}_1$ can be discontinuous across the interface, double nodal values of $\boldsymbol{\tau}_1$ are defined at each interfacial node. For pressure, we use first-order shape functions of class C^{-1}; this interpolation makes possible a pressure discontinuity at the interface. Note that the equilibrium condition (14) is satisfied in the Galerkin sense through (16).

The computation of the interface location remains to be discussed. For the case of co-flow of two Newtonian fluids solved with the velocity–pressure formulation, we adopt the coupled approach developed by Kistler and Scriven [6]. The location of interfacial nodes is determined by means of pre-defined spines and unknown nodal coefficients h_i. Each spine is defined by a base point $\boldsymbol{x}_{\mathrm{B}}^i$ and a direction vector $\boldsymbol{e}_i$; the position of interfacial node P_i is then given by

$$\boldsymbol{x}(P^i) = \boldsymbol{x}_{\mathrm{B}}^i + h_i \boldsymbol{e}_i. \tag{19}$$

Nodes that do not lie on the interface must also belong to a spine; the position vector of such a node P^m is thus given by a relation of the form

$$\boldsymbol{x}(P^m) = \boldsymbol{x}_{\mathrm{B}}^i + C^m h_j \boldsymbol{e}_j, \tag{20}$$

where C^m is a constant. The displacement of the finite element nodes in the iterative process is thus anchored to that of the interface in a way that

preserves the initial topology of the elements layout. In order to compute the coefficient h_i, we impose the kinematic condition (11) in the Galerkin sense, i.e.

$$\int_\Gamma \beta_1 [\boldsymbol{v}^\alpha \cdot \boldsymbol{n}^\alpha] \, \mathrm{d}\Gamma = 0, \tag{21}$$

where the β_1's are one-dimensional quadratic shape functions. Equations (16), (18) and (21) constitute in the Newtonian case a set of nonlinear algebraic equations for the velocity, pressure and interface nodal values. In compact form we have

$$\boldsymbol{A}(\boldsymbol{v}_i^\alpha, \, p_k^\alpha, \, h_1) = \boldsymbol{0}. \tag{22}$$

We solve (22) by means of Newton–Raphson's iterative scheme. The computation of the Jacobian matrix components $\partial A_i / \partial h_j$ is very tedious but straightforward.

The coupled approach described above can also be used when the co-flowing fluids are viscoelastic [11]. Derivation of the corresponding Jacobian matrix is, however, very lengthy since the discretized constitutive equations (17) are now part of the final algebraic system. In this work, we have adopted a simpler Picard iterative scheme to update the location of the interface when at least one of the two fluids is viscoelastic. Equations (16)–(18) are solved on a fixed mesh for the nodal values of τ_1^α, $\boldsymbol{v}^\alpha$ and p^α by means of Newton's method. The newly-computed velocity field is then used to integrate the kinematic condition (11) in its differential form [5]:

$$v_z \, \mathrm{d}r - v_r \, \mathrm{d}z = 0, \qquad \boldsymbol{x} \in \Gamma. \tag{23}$$

where v_r and v_z are the radial and axial velocity components, respectively (Fig. 1). Finally, the internal nodes are displaced in the manner prescribed by (20), and the process is repeated until convergence. This simple scheme has been found to be quite satisfactory in our co-flow simulations. Its convergence behavior is linear and indeed similar to that found in extrusion flow calculations [5,9].

4. Flow parameters and boundary conditions

The numerical technique has been used to simulate co-flow experiments conducted by Van de Griend and Denn [10]. These authors studied co-current flows through axisymmetric sudden expansions or contractions involving two immiscible Newtonian or viscoelastic fluids. Newtonian fluids used in the experiments were silicone oils and corn syrups, while the viscoelastic liquids were dilute solutions of polyacrylamide in corn syrup. The numerical simulations reported below correspond to the experiments carried out with

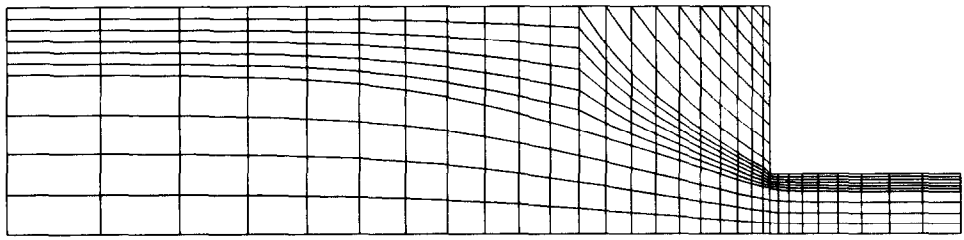

Fig. 2. A typical finite element mesh used in co-flow simulations.

the silicone oils SF96-1000 and Viscasil 10 000, and the polymer solutions C13PA-E and C130PA-E; these fluids are characterized in Table 1 of [10].

A schematic of the flow geometry is given in Fig. 1 for the case of a 1 : 4 sudden expansion. In both Newtonian/Newtonian and viscoelastic/viscoelastic computations, the more viscous fluid flows in the core of the expansion while the less viscous fluid is in contact with the expansion wall. The boundary conditions are as follows:

(i) fully-developed velocity and viscoelastic extra-stress profiles at the flow inlet,
(ii) no-slip condition at the die wall,
(iii) fully-developed flow conditions at the flow outlet, and
(iv) symmetry conditions along the axis of symmetry.

The boundary condition (iii) is specified in terms of radial velocity and axial traction in the Newtonian case; both radial and axial velocity components are specified in the viscoelastic case. The flow rate of each fluid phase (and thus the inlet interface location) is assigned the dimensional value set in the experiments [10].

Figure 2 shows a typical finite element mesh used in the computations. Mesh refinement is needed close to the wall (i.e. in the less viscous fluid phase) to capture the larger stress and velocity gradients. The spines used in the interface calculation are lines of constant axial position. Typical Newtonian simulations involved about 2500 degrees of freedom and required of the order of 10 seconds of CRAY X-MP CPU time per Newton iteration. The corresponding figures for viscoelastic runs are 5500 degrees of freedom and 20 CPU seconds (per Picard iteration).

5. Results

5.1 Newtonian / Newtonian

Numerical results for the two silicone oils are compared to the experimental observations in the companion paper [10]. Inner to outer fluid flow rate

ratio is equal to 3.8. The large viscosity ratio between the two fluids (i.e. 8.5 in the present case) gives rise to significant corner vortex activity in the less viscous fluid phase. Agreement between observed and computed streamlines is excellent. There is, however, a small but systematic deviation between measured and predicted axial velocity developments [10]. A possible cause is a magnification of the slight asymmetry of the experimental flows resulting from sensitivity to small changes in the interface location. Indeed, one side of the streakline photograph taken by Van de Griend and Denn gives an estimated value of 0.56 for the dimensionless vortex reattachment length L/D (Fig. 1), while the other side of the same photograph yields 0.68. Numerical experiments with successively refined meshes give a value of 0.60 for L/D.

5.2 Viscoelastic / Viscoelastic

Viscoelastic computations were conducted to simulate the experiments of Van de Griend and Denn [10] with the polyacrylamide solutions C13PA-E (outer fluid) and C130PA-E (inner fluid). The elasticity data for the outer fluid are $\lambda_p = 0.15$ s and $\lambda_r = 0.09$ s, while those for the inner fluid are $\lambda_p = 1.6$ s and $\lambda_r = 1$ s. The inner to outer fluid viscosity and flow rate ratios are 10 and 1.81, respectively. The experimental flow parameters are such that the outer fluid can be considered as Newtonian [10]. Our numerical results with the outer fluid taken as a Newtonian or an Oldroyd-B fluid produced virtually identical results. The Weissenberg number We, as defined by eqn. (5b) of [10], is equal to 0.14 for both expansion and contraction flows. This corresponds to a value of 3.7 if one uses the definition of We adopted by Dheur and Crochet [11], i.e.

$$We = \lambda_p V_1 / R_1, \tag{24}$$

where R_1 is the radius of the inner fluid core in the small diameter tube and V_1 is the corresponding average velocity. Experimental observations reported in [10] show only small viscoelastic effects on the flow kinematics for that value of We. The same is true of the present numerical simulations.

Figure 3 shows a comparison between experimental and computed streamlines for the case of expansion flow. Agreement is excellent. A large corner vortex is present in the quasi-Newtonian fluid phase, due to the high viscosity ratio. Profiles of axial and radial velocity components obtained downstream of the expansion plane are given in Fig. 4. As in the Newtonian case, agreement between predicted and observed velocity profiles is good, even though there is a systematic deviation possibly due to the slight asymmetry of the experimental flow field. The predicted interface location is clearly marked in Fig. 4 by a discontinuity in the velocity gradient. Com-

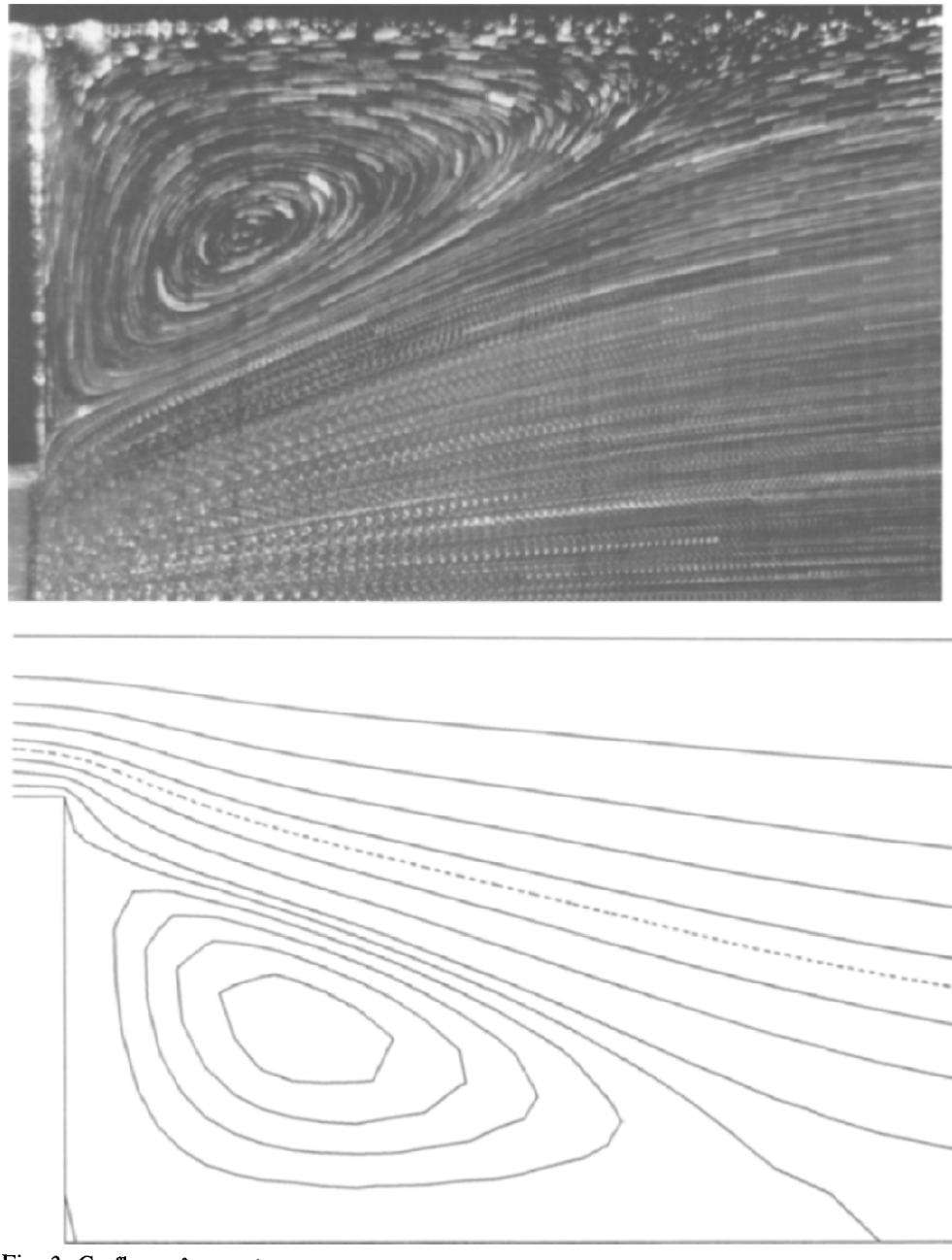

Fig. 3. Co-flow of two viscoelastic fluids through an abrupt expansion; experimental flow field [10] and streamlines computed with the Oldroyd-B model. The dashed line denotes the predicted interface.

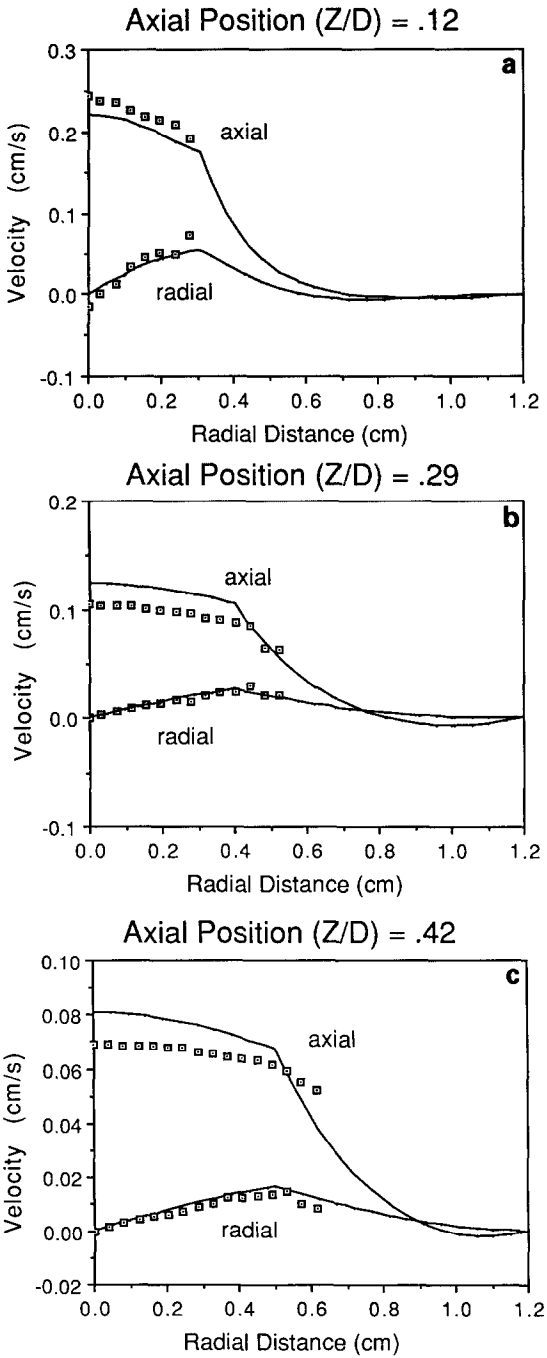

Fig. 4. Axial and radial velocity components in co-flow through an abrupt expansion; experimental data points [10] and numerical predictions based on the Oldroyd-B model.

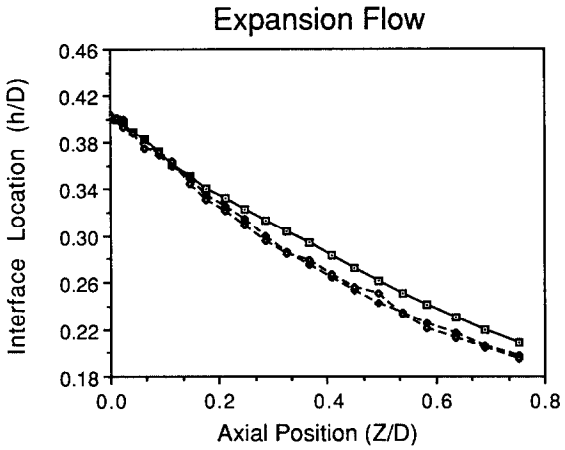

Fig. 5. Interface development in co-flow through an abrupt expansion; experimental data for both sides of the laser specklegram [10] (◆——◆ Left, ◇——◇ Right) and numerical prediction based on the Oldroyd-B model (⊡——⊡). The symbol h denotes the radial distance between the interface and the die wall.

puted and observed interface developments in the expansion region compare rather well, as shown in Fig. 5.

Identical conclusions can be drawn with our co-flow simulations of the same two fluids through an abrupt 4:1 contraction. Figure 6 shows a comparison between predicted and observed streamlines. There is only a small difference in the computed interface curvature between expansion and contraction flows at this elasticity level. The vortex strength, however, is 28% higher for the contraction flow. A comparison between observed and computed velocity components upstream of the contraction plane is given in Fig. 7. Note that numerical results are shown at three slightly different axial positions such as to take into account the 4% experimental uncertainty in the axial position of the contraction plane. Interface development in the contraction region is depicted in Fig. 8. Agreement with the experimental data is excellent.

5.3 High elasticity results

The above viscoelastic simulations were carried out further at elasticity levels beyond the range covered by the experiments of Van de Griend and Denn. The relaxation time λ_p of the inner fluid was increased from 1.6 s to 15 s, all other material and flow parameters being kept constant. The highest value for the relaxation time corresponds to $We = 1.2$ with the definition used in [10], or $We = 34$ with that of eqn. (24). Pursuing the computations to higher elasticity levels did not seem to be difficult but would have required

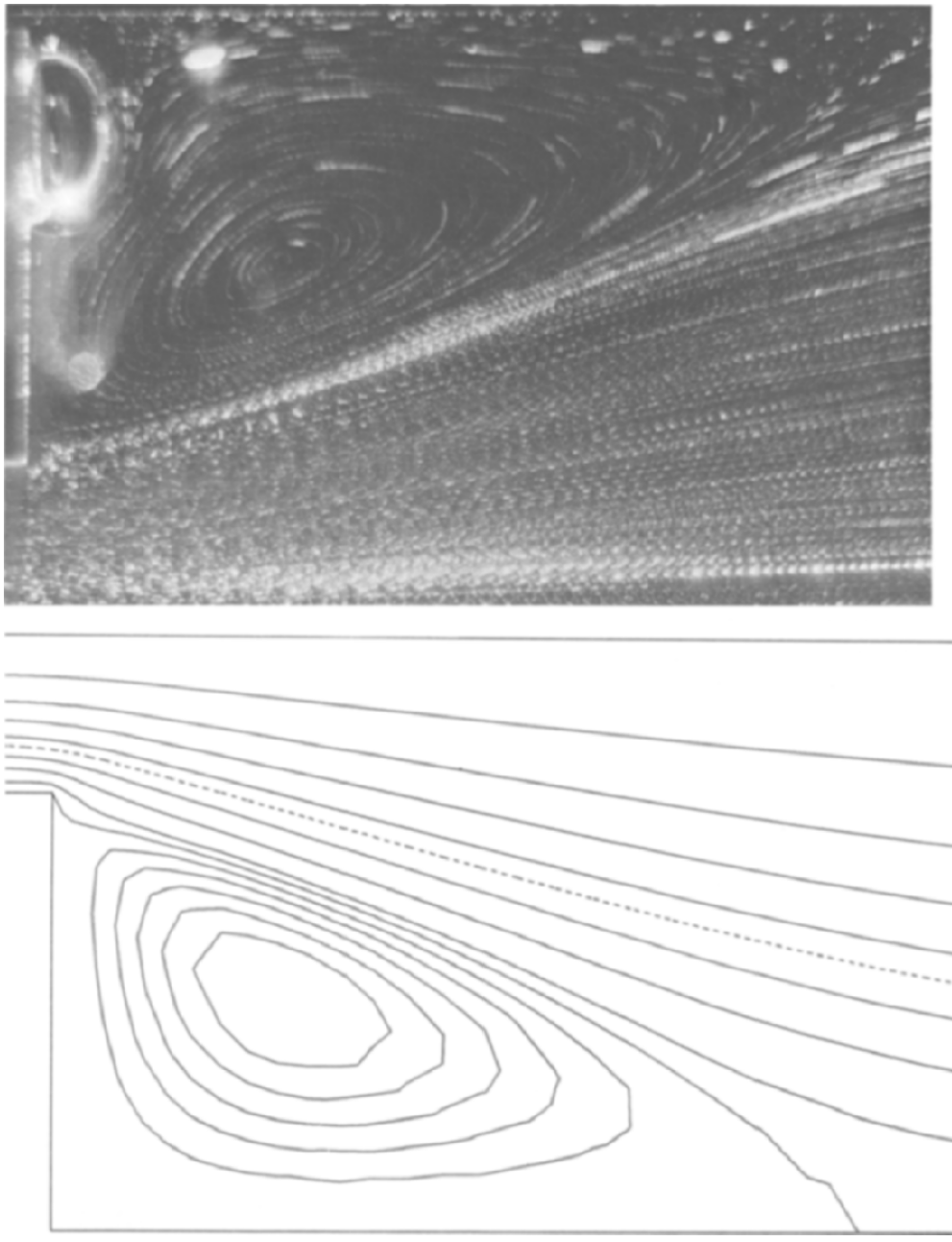

Fig. 6. Co-flow of two viscoelastic fluids through an abrupt contraction; experimental flow field [10] and streamlines computed with the Oldroyd-B model. The dashed line denotes the predicted interface.

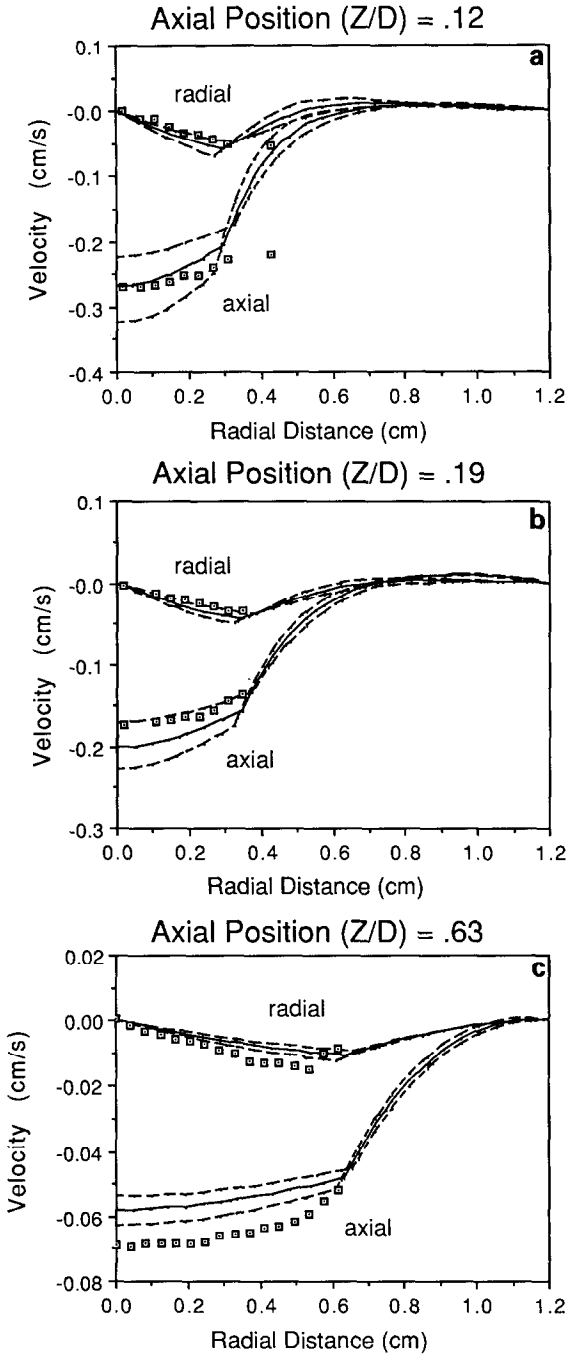

Fig. 7. Axial and radial velocity components in co-flow through an abrupt contraction; experimental data points [10] and numerical predictions based on the Oldroyd-B model.

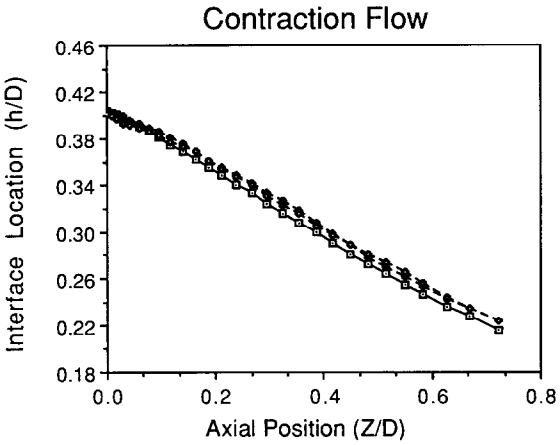

Fig. 8. Interface development in co-flow through and abrupt contraction; experimental data for both sides of the laser specklegram [10] (◆——◆ Left; ◇——◇ Right) and numerical predictions based on the Oldroyd-B model (⊡——⊡). The symbol h denotes the radial distance between the interface and the die wall.

the use of very long (and thus expensive to discretize) exit regions in order to allow the viscoelastic stress field to reach a fully-developed profile. Success of these highly elastic flow simulations is undoubtedly due to the presence of a Newtonian fluid phase adjacent to the expansion wall which renders the corner stress singularity both more physically reasonable and numerically tractable than in single-viscoelastic fluid flow calculations [7].

Figure 9 shows, in the case of expansion flow, the predicted interface locations and recirculation zones for $\lambda_p = 1.6$ s and 15 s. The interface reaches its fully-developed location more rapidly as elasticity of the inner fluid increases. This trend is accompanied by a significant decrease in vortex strength and reattachment length with increasing inner fluid elasticity. Predicted vortex size and strength are shown in Fig. 10 as a function of the inner fluid relaxation time. There is an initial increase at low elasticity levels, followed by a monotonic decrease beyond some critical value of the inner fluid relaxation time. Numerical experiments with various viscosity ratios

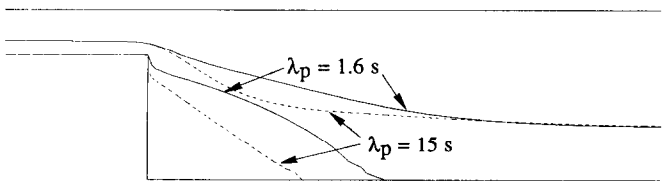

Fig. 9. Influence of inner fluid elasticity on interface location and recirculation zone in co-flow through an abrupt expansion; numerical predictions based on the Oldroyd-B model.

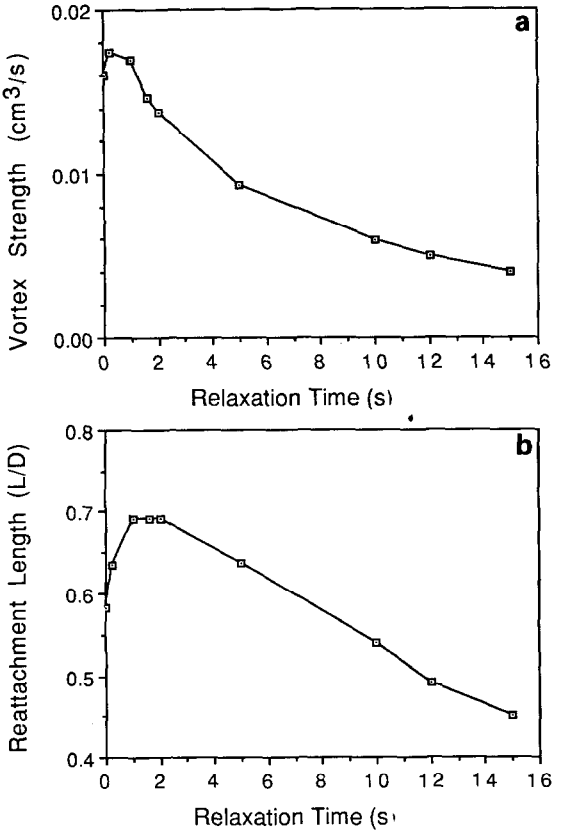

Fig. 10. (a) Vortex strength and (b) reattachment length as a function of inner fluid elasticity in co-flow through an abrupt expansion; numerical predictions based on the Oldroyd-B model.

indicate that existence of the initial increase in the vortex characteristics curves only occurs for sufficiently high viscosity ratios. Viscoelastic effects on co-flow kinematics similar to those described in this section have been computed recently by Dheur and Crochet [11] with the upper-convected Maxwell fluid.

6. Conclusions

We have presented a finite element technique for solving the steady-state co-flow of two immiscible viscoelastic fluids in complex geometries. Numerical predictions for both Newtonian and viscoelastic co-flows through abrupt expansions and contractions are in good agreement with the detailed experimental observations of Van de Griend and Denn [10]. Results for a highly

elastic inner fluid lubricated by a virtually Newtonian outer layer reveal important kinematic differences relative to the Newtonian case.

Acknowledgments

This work was supported by the Director, Office of Energy Research, Office of Basic Energy Sciences, Materials Science Division of the U.S. Department of Energy under Contract No. DE-ACO3-76SF00098. The numerical simulations described in this paper have been conducted on a CRAY X-MP supercomputer of the National Magnetic Fusion Energy Computer Center, Lawrence Livermore National Laboratory.

References

1 E. Mitsoulis, J. Rheol., 30 (1986) 23.
2 H. Mavridis, A.N. Hrymak and J. Vlachopoulos, AIChE J., 33 (1987) 410.
3 D.M. Binding, K. Walters, J. Dheur and M.J. Crochet, Phil. Trans. R. Soc. London, A323 (1987) 449.
4 J. Dheur and M.J. Crochet, Rheol. Acta, 26 (1987) 401.
5 R.E. Nickell, R.I. Tanner and B. Caswell, J. Fluid Mech., 65 (1974) 189.
6 S.F. Kistler and L.E. Scriven, Coating flows, in: J.R.A. Pearson and S.M. Richardson (Eds.), Computational Analysis of Polymer Processing. Elsevier Applied Science, London, 1983, p. 243.
7 R. Keunings, Simulation of viscoelastic fluid flow, in: C.L. Tucker III (Ed.) Fundamentals of Computer Modeling for Polymer Processing. Carl Hanser Verlag, Munich, in press (1989)
8 M.J. Crochet, Numerical Simulation of Viscoelastic Flow: a Review, Am. Chem. Soc., Rubber Chem. Technol., (Rubber Reviews), in press (1989)
9 M.J. Crochet and R. Keunings, J. Non-Newtonian Fluid Mech., 10 (1982) 339.
10 R. van de Griend and M.M. Denn, J. Non-Newtonian Fluid Mech., 32 (1989) 229.
11 J. Dheur and M.J. Crochet, J. Non-Newtonian Fluid Mech., 32 (1989) 1.